Arch. Mech., 34, 4, pp. 503–514, Warszawa 1982

On experimental two-dimensional models of intercrystalline sliding and fracture in polycrystalline metals(*)

W. SZCZEPIŃSKI (WARSZAWA)

SIMPLE experimental models of polycrystalline structure of metals composed of rigid hexagonal elements forming a regular aggregate are proposed in order to simulate intercrystalline sliding and fracture. The grain boundaries are simulated by layers of solid lubricate between adjacent hexagons or by rows of holes prepared in a solid block of a ductile metal. The behaviour of these models is compared with the properties of an analogous theoretical model.

Rozpatrzono proste doświadczalne modele struktury polikrystalicznej złożone ze sztywnych sześciokątnych elementów tworzących regularny układ. Modele te symulują międzykrystaliczne poślizgi i pękanie w metalach. Granice ziaren są w tych modelach symulowane przez warstwy stałego smaru umieszczonego między sąsiednimi sześciokątami, albo przez szeregi otworów wykonanych w bloku z ciągliwego metalu. Zachowanie się tych modeli porównano z własnościami analogicznego modelu teoretycznego.

Рассмотрены простые экспериментальные модели поликристаллической структуры, состоящие из жестких шестиугольных элементов, образующих регулярную систему. Эти модели имитируют межкристаллические скольжения и растрескивания в металлах. Границы зерен в этих моделях имитируются слоями твердой смазки, помещенной между соседними шестиугольниками, или рядами отверстий, изготовленных в блоке из тягучего металла. Поведение этих моделей сравнено со свойствами аналогичной теоретической модели.

1. Introduction

THE PHENOMENA of plastic deformation and fracture of polycrystalline metals are very complex and still not fully examined. Depending on the temperature and the rate of deformation, various mechanisms of deformation may be responsible for the particular behaviour of the material under given circumstances. Grain interior deformation and grain boundary sliding may contribute to the plastic strain of the polycrystalline aggregate, while transgranular fracture or intercrystalline void formation may lead to the fracture of the aggregate. The mechanism of intergranular fracture has been widely discussed in papers devoted to the creep phenomenon in metals (see [1, 2]). However, it is observed (see for example [3]) that in some alloys the generation of grain boundary cavities is connected with the plastic strain and not necessarily with the creep deformation. For example, intergranular fracture has been observed in wolfram tested in simple tension at the temperature of 2200°C [4].

In order to obtain a deeper insight into the mechanism of the formation of intercrystalline voids and of plastic deformation of the polycrystalline aggregate due to grain

(*) The paper was presented at the IUTAM Symposium on Crack Formation and Propagation held in Tuczno (Poland) on March 23–27, 1981.

boundary sliding, two-dimensional models were considered in several works, for example in [5, 6]. These works were devoted to the analysis of the growth of grain boundary cavities during creep and were connected with the diffusional cavity growth rates. A similar model was used in [7], for the analysis of strength of sintered carbides.

In the present work similar two-dimensional models composed of rigid hexagonal elements will be used in order to study possible mechanisms of plastic deformation of polycrystalline aggregates due to grain boundary sliding and intercrystalline void formation leading to the softening of the plastically deformed aggregate.

2. Experimental model of intercrystalline sliding and fracture

The possible role of intercrystalline sliding and fracture can be demonstrated to some extent with the simple two-dimensional model composed of rigid hexagons joined together by layers of solid silicon lubricate (Fig. 1a), and located on a glass plate. In order to avoid

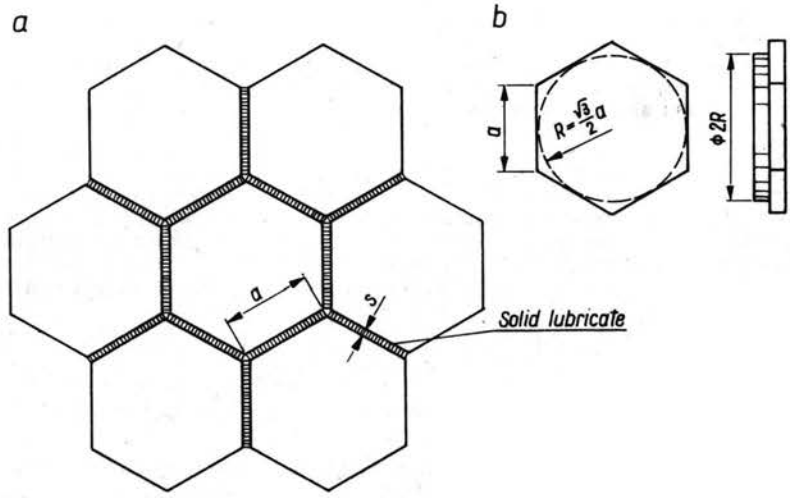

FIG. 1.

contact of the lubricate with the plate, the hexagons were designed in the manner shown in Fig. 1b. Their cylindrical part (of the radius $R = a\sqrt{3}/2$) was in contact with the plate. Since the thickness s of the layer of the lubricate is small as compared with the length a of the side of each hexagon, the models simulate to a certain degree grains and grain boundaries of a polycrystalline aggregate.

Consecutive stages of deformation of the model under compression followed by tension are shown in Fig. 2. Figure 2a shows the initial configuration when hexagons are joined together by the thin layers of the lubricate along all five contact edges. The three following sketches demonstrate how a gap along the vertical boundary AB (Fig. 2d) is formed after the loading cycle. The adhesion of the lubricate was not restored along AB, while along the remaining four inclined boundaries the adhesion was not damaged by the relative sliding of the hexagons. Thus the sliding process along these boundaries is kinematically reversible, while along AB the process of separation is irreversible.

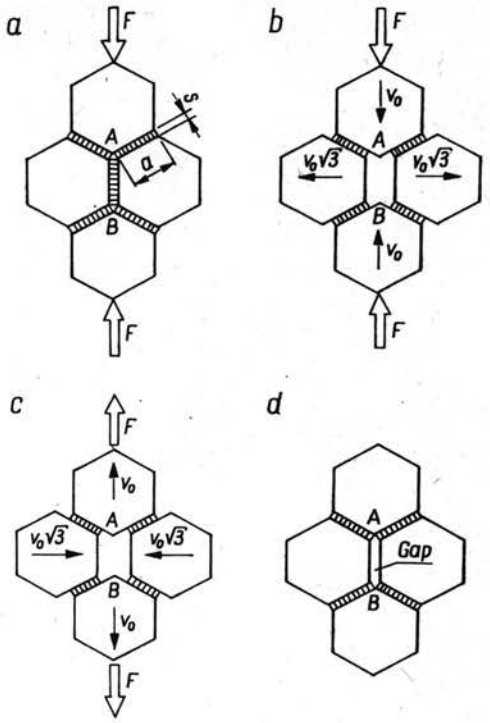

FIG. 2.

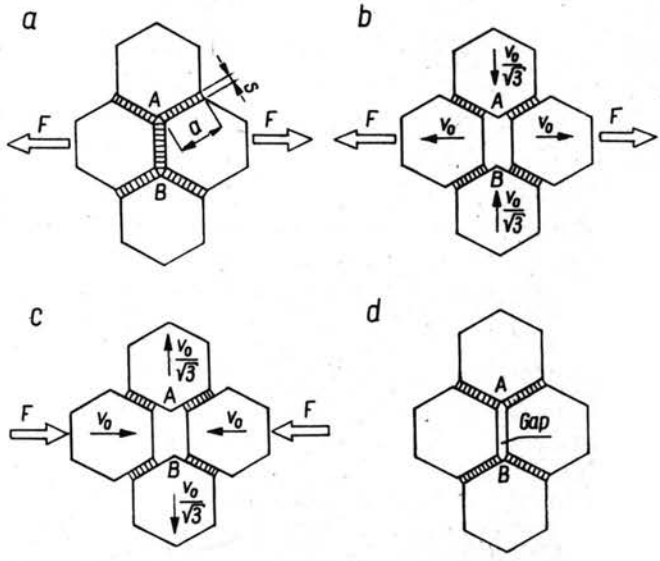

FIG. 3.

In a similar way a crack along AB is formed during the loading by tension in a horizontal direction followed by compression in the same direction (Fig. 3) (1).

3. Theoretical model of intercrystalline sliding and fracture

Let us consider now a theoretical model forming a regular array composed of n hexagons in horizontal rows and m hexagons in vertical rows as shown in Fig. 4a (in the particular case shown in the figure we have $m = n = 3$). As in the previous experimental

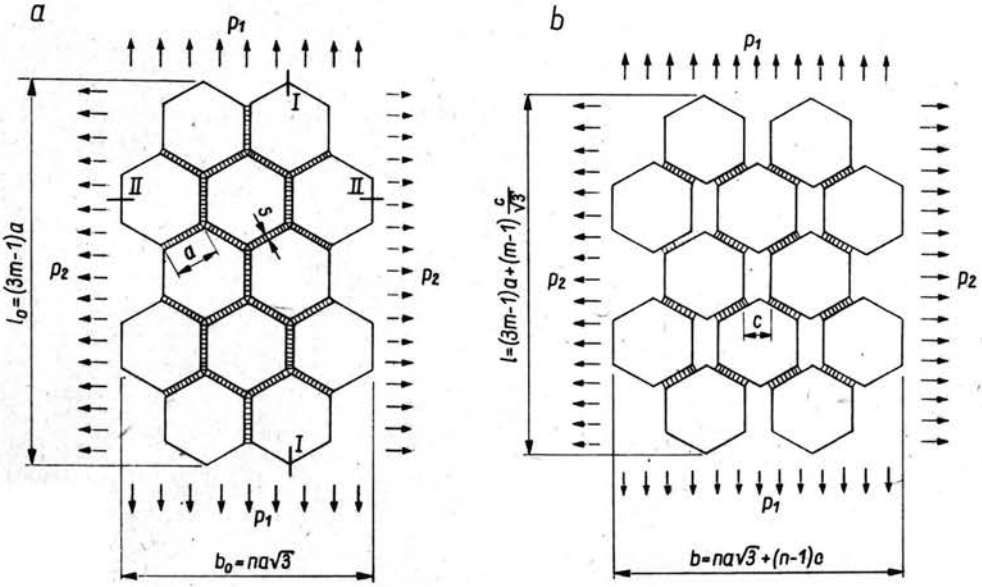

FIG. 4.

model, the hexagons are assumed to be joined together by thin layers of thickness s simulating the grain boundaries. Let the model be loaded by the two-dimensional state of stresses p_1 and p_2 such that deformation of the type shown in Fig. 4b takes place.

The hexagons are taken as rigid and the ratio s/a is assumed to be small. The material of the layers between hexagons is taken as rigid-plastic. Figure 5 presents in enlarged scale a configuration of four hexagons after deformation, defined by the distance c between vertical edges ($c > s$). Let us assume that inside each layer between the hexagons there exists a system of voids or cracks perpendicular to the edge of the respective hexagon. Thus the layer may be treated as a system of discontinuous individual elements of limited strength in tension. Therefore the stress along the boundary AB perpendicular to the direction of elongation of the aggregate may be taken as uniformly distributed up to the limit value c_0 of the distance c between the edges of the two adjacent hexagons by which

(1) Such processes of deformation of the model have been demonstrated with the use of an overhead projector at the IUTAM Symposium on Crack Formation and Propagation held in Tuczno Poland on March 23—27, 1981, and at the 3rd International Seminar on Inelastic Analysis and Life Prediction held in Paris, August 24—25, 1981.

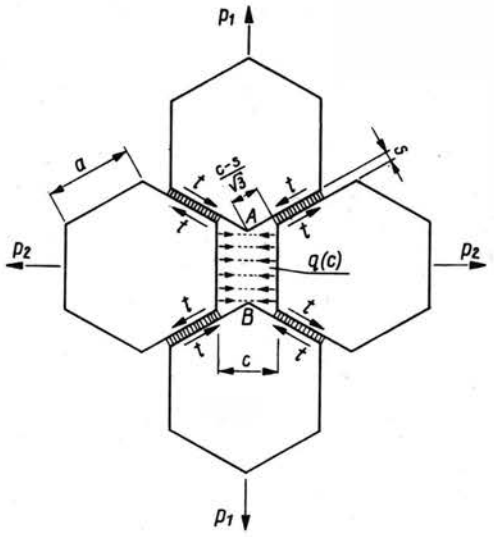

FIG. 5.

the cohesion forces decrease to zero. This means that at $c = c_0$ total separation along AB takes place. Let $q(c)$ be the cohesive force per unit length along AB for $s \leqslant c \leqslant c_0$. Now we can write the expression for the specific energy γ required to separate adjacent hexagons along AB:

$$\gamma = \int_s^{c_0} q(c)\,dc.$$

Along the inclined surfaces shear deformation takes place as shown in Fig. 5. The shear strain in each of the inclined layers may be approximately defined as

$$\lambda = \frac{1}{2}\frac{c-s}{s\sqrt{3}} = \frac{1}{2\sqrt{3}}\left(\frac{c}{s}-1\right).$$

Thus it is equal to one half of the shear angle $(c-s)/(s\sqrt{3})$. This shear strain in the inclined layer is directly connected with the average strain ε_2 of the model in the horizontal direction. The relation between λ and ε_2 resulting from geometrical considerations may be written as

$$\varepsilon_2 = \frac{c-s}{s+a\sqrt{3}} = 2\lambda\varkappa, \tag{2.1}$$

where

$$\varkappa = \frac{\sqrt{3}\,s}{s+a\sqrt{3}} \approx \frac{s}{a} \tag{2.2}$$

is a structural parameter of the model.

Let us assume a linear strain hardening relation between the shear stress t on the inclined surface of each hexagon and the average strain ε_2 in the form

$$t = t_0(1+r\varepsilon_2), \tag{2.3}$$

where $r = t_1/t_0$ is the strain hardening factor of layers undergoing shear deformation (see Fig. 6).

Now we can write the equation of virtual work, which for $s \leqslant c < c_0$ may be written as

$$p_2 l_0(n-1)\Delta c - p_1 b_0 \frac{\Delta c}{\sqrt{3}} = [m(n-2)+(m-1)(n-1)]aq(c)\Delta c + 4(m-1)(n-1)\frac{\Delta c}{\sqrt{3}} t_0(1+r\varepsilon_2)\left(a-\frac{c-s}{\sqrt{3}}\right), \tag{2.4}$$

where, according to Fig. 4a, we have

$$l_0 = a(3m-1), \quad b_0 = na\sqrt{3}. \tag{2.5}$$

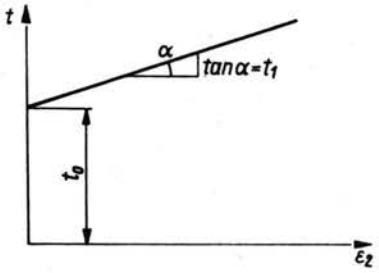

FIG. 6.

For simplicity the latter expression for l_0 and b_0 have been written ignoring the thickness s of the layers between hexagons. Since s is very small compared with the length of the side of hexagons, such a simplification is justified.

Introducing Eq. (2.5) into Eq. (2.4) we obtain the yield condition for the initial stage of deformation of the model (for $s \leqslant c < c_0$):

$$p_2(3m-1)(n-1)-p_1 n(m-1) = [m(n-2)+(m-1)(n-1)]q(c) + \frac{4}{\sqrt{3}}(m-1)(n-1)(1+r\varepsilon_2)\left(1-\frac{s}{\varkappa a}\varepsilon_2\right)t_0. \tag{2.6}$$

The cohesion force per unit length along AB changes its value from q_0 at the beginning of the deformation process ($c = s$) to zero for $c = c_0$. Therefore the right hand side of the yield condition (2.6) changes its value from

$$[m(n-2)+(m-1)(n-1)]q_0 + \frac{4}{\sqrt{3}}(m-1)(n-1)(1+r\varepsilon_2)\left(1-\frac{s}{\varkappa a}\varepsilon_2\right)t_0$$

for $c = s$, to the value

$$\frac{4}{\sqrt{3}}(m-1)(n-1)(1+r\varepsilon_2)\left(1-\frac{s}{\varkappa a}\varepsilon_2\right)t_0$$

for $c = c_0$. Thus our model displays the phenomenon of the upper and lower yield point at the beginning of deformation. This will be shown later on in Fig. 9 in which the stress-strain diagram for uniaxial tension by the stress p_2 is presented.

At the moment when $c = c_0$ the yield condition may be written in the approximate form

$$p_2 - p_1 \frac{n(m-1)}{(3m-1)(n-1)} = \frac{4}{\sqrt{3}} \frac{m-1}{3m-1} t_0. \tag{2.7}$$

Assuming that c_0 is small, we neglect the small amount of hardening in the inclined contact layers.

Equation (2.7) shows how strongly the yield locus of the model depends on the number of hexagons forming the aggregate. For uniaxial tension by the stress p_2 we obtain

$$p_2 = \frac{4}{\sqrt{3}} \frac{m-1}{3m-1} t_0. \tag{2.8}$$

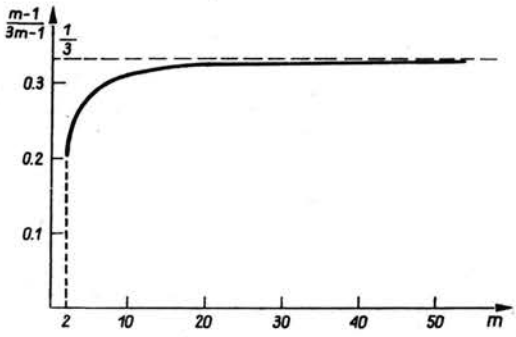

FIG. 7.

Figure 7 shows how the factor $(m-1)/(3m-1)$ changes with the increasing number m of hexagons in vertical rows. It is clearly seen that the larger the number of hexagons, the higher the yield point of the aggregate. So if we compare two aggregates of the same external dimensions, the one composed of a larger number of hexagons with small length of the side a will be stronger than the other composed of a smaller number of larger hexagons. This corresponds to the well-known property of technical metals. Structures of metals with fine grains behave better than those with coarse grains.

The yield condition (2.7) is presented on the stress plane p_1, p_2 in Fig. 8. The lower line corresponds to the smallest possible number of hexagons forming the model ($n = 2$, $m = 2$), while the upper line corresponds to $m = n = \infty$.

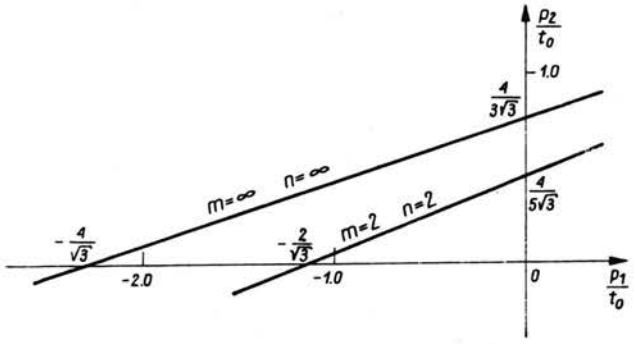

FIG. 8.

For the advanced stage of deformation (for $c > c_0$) the equation of virtual work takes the form

$$(2.9)\quad p_2 l(n-1)\Delta c - p_1 b(m-1)\frac{\Delta c}{\sqrt{3}} = 4(m-1)(n-1)\frac{\Delta c}{\sqrt{3}}\, t_0(1+r\varepsilon_2)\left(a-\frac{c-s}{\sqrt{3}}\right),$$

where, according to Fig. 4b,

$$l = a(3m-1)+(m-1)\frac{c}{\sqrt{3}}, \qquad b = na\sqrt{3}+(n-1)c.$$

Thus the yield condition for the advanced stage of deformation is

$$(2.10)\quad p_2\left[(3m-1)+(m-1)\frac{1}{\sqrt{3}}\frac{c}{a}\right](n-1)$$
$$-p_1\left[n\sqrt{3}+(n-1)\frac{c}{a}\right](m-1)\frac{1}{\sqrt{3}} = \frac{4}{\sqrt{3}}(m-1)(n-1)(1+r\varepsilon_2)\left(1-\frac{s}{\varkappa a}\varepsilon_2\right) t_0.$$

Taking into account Eqs. (2.1) and (2.2), we can write

$$\frac{c}{a} \approx (\varkappa+\sqrt{3})\,\varepsilon_2+\varkappa.$$

Since $\varkappa$ is small as compared with $\sqrt{3}$, we can write with sufficient accuracy

$$\frac{c}{a} \approx \sqrt{3}\,\varepsilon_2.$$

Finally the yield condition (2.10) may be written in the following approximate form:

$$(2.11)\quad p_2-\frac{1}{n-1}\,\frac{[n+(n-1)\varepsilon_2](m-1)}{(3m-1)+(m-1)\varepsilon_2}\,p_1 = \frac{4}{\sqrt{3}}\,\frac{(m-1)(1+r\varepsilon_2)(1-\varepsilon_2)}{(3m-1)+(m-1)\varepsilon_2}\,t_0.$$

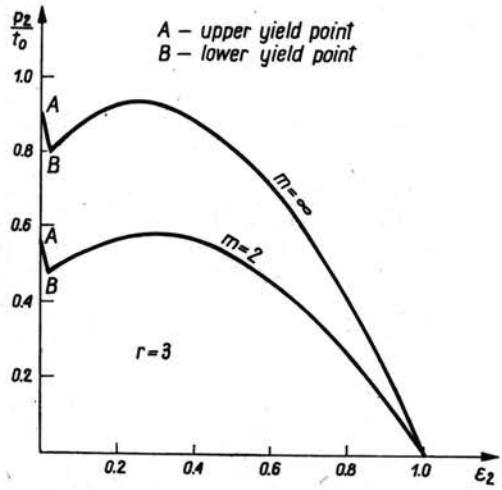

FIG. 9.

Let us consider a particular case of uniaxial tension by the stresses p_2. Thus, from Eq. (2.11) we obtain the relation

$$p_2 = \frac{4}{\sqrt{3}} \frac{(m-1)(1+r\varepsilon_2)(1-\varepsilon_2)}{(3m-1)+(m-1)\varepsilon_2} t_0,$$

which is graphically presented in Fig. 9 for $r = 3$ and for the numbers of hexagons $m = 2$ and $m = \infty$, respectively. These stress-strain diagrams display two kinds of instability. At the beginning of the diagrams there appears a remarkable sudden drop of stresses connected with the decohesion process along the vertical boundaries between hexagons. The second type of instability appearing at the advanced stage of deformation results from the instability of the shearing process along inclined boundaries.

4. Another experimental model of intercrystalline sliding and fracture

In the second type of the experimental model of intercrystalline sliding and fracture, the grain boundaries are simulated by the rows of holes prepared in a block of a ductile aluminium alloy PA2N (with content of ca 2% of Mg). A simple experimental setup is shown in Fig. 10. The block is compressed between two steel platens.

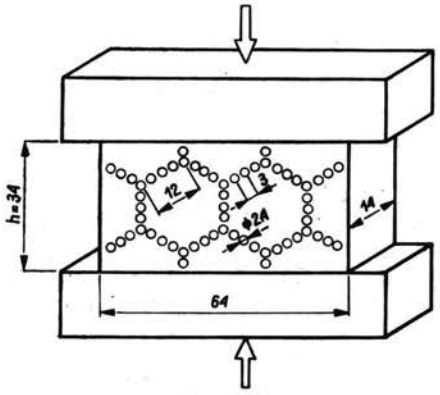

FIG. 10.

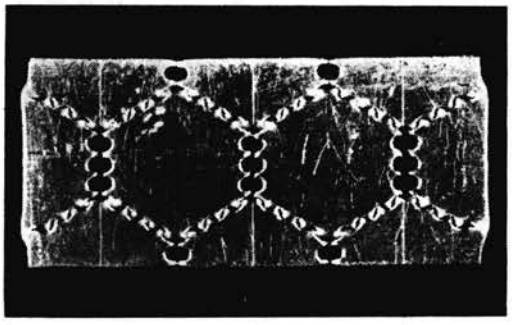

FIG. 11.

The block deformed up to the permanent strain $\varepsilon_p = 10.3\%$ in the vertical direction is shown in Fig. 11. Total separation of ligaments between the holes along the vertical rows is clearly visible. There is no such decohesion along inclined rows of holes where strong shear deformation only is observed. Thus the present experimental model behaves similarly as the first experimental model shown in Fig. 2.

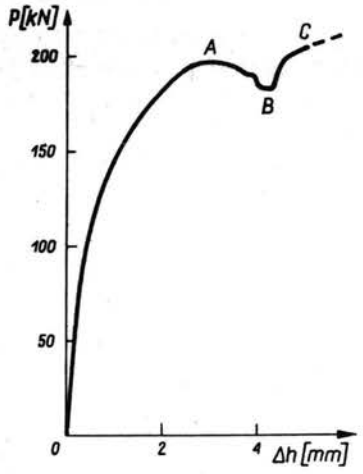

FIG. 12.

In the force-elongation diagram shown in Fig. 12 there appears clearly visible instability between the points A and B. This instability is connected with the process of decohesion along the vertical rows of holes. After the total separation along these vertical rows, the compressive force increases. This must be attributed to the hardening along the inclined rows of holes connected with the complex process of shearing.

A similar type of instability between the points A and B appeared in the stress-strain piagram (Fig. 9) calculated for the theoretical model discussed in the previous section.

The deformation mode shown in Fig. 11 takes place if the simulated grain boundaries are sufficiently "weak" or, in other words, if the diameter of holes is sufficiently large as compared with the spacing between the holes. Dimensions for the present case have been shown in Fig. 10. The ratio $\xi = 1 - \frac{d}{c}$ (ligament width/spacing between holes) was equal to 0.2. For example, tested specimens with this ratio equal to 0.4 displayed a completely different mode of deformation consisting in the plastic deformation of "grains" and simultaneous plastic deformation of "boundaries". No decohesion along vertical boundaries was observed. Thus our simple experimental model demonstrates how the possibility of intercrystalline fracture of plastically-deformed polycrystalline metals depends on the "toughness" of grain boundaries.

The effect of the ratio ξ is less visible in models pulled in tension. Figure 13a shows a simple tension specimen with prepared rows of holes and the ratio $\xi = 0.47$. In the fractured specimen, after the test (Fig. 13b), a wide gap along the row of holes perpendicular to the tension direction is visible. During the fracture precess decohesion along this row of holes is followed by a combined shearing-tensile fracture along inclined rows of

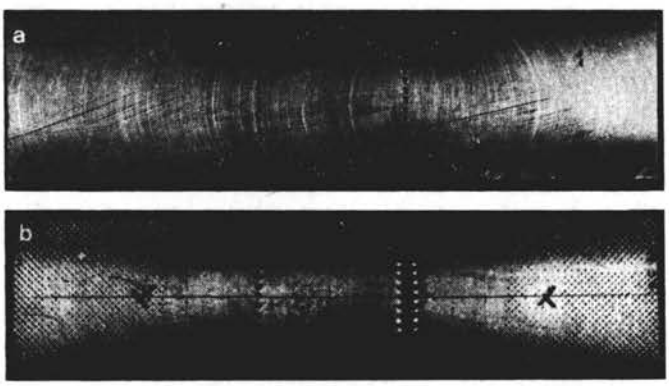

FIG. 13.

holes. Such a sequence of various mechanisms of fracture along differently-oriented "grain boundaries" leads finally to the total separation of the two parts of the specimen.

Another type of perforated tensile specimens is shown in Fig. 14. In order to obtain a smoother course of final stage of the fracture process in the central perforated part,

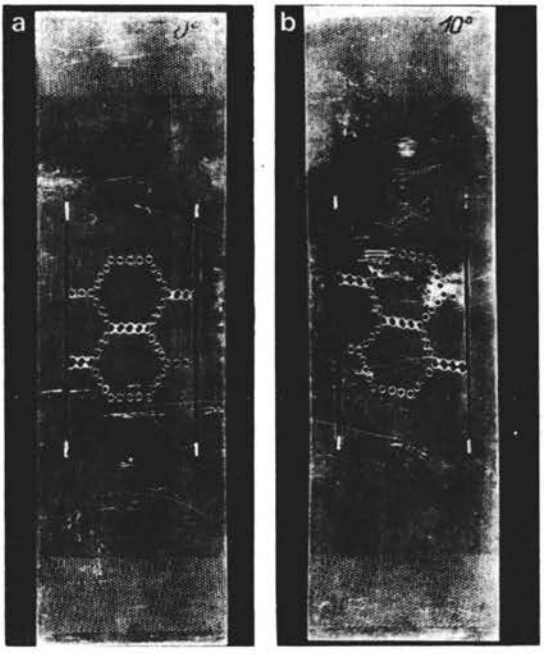

FIG. 14.

each specimen has two-side strips. These strips assure the quasi-static run of the final stage of the fracture process even with the use of the standard ordinary hydraulic testing machine. In Fig. 14a we can observe decohesion along the rows of holes perpendicular to the tension direction and advanced shearing without fracture along inclined rows of holes. The same mode of fracture and deformation takes place in the case when the rows

of holes undergoing fracture are slightly inclined as shown in Fig. 14b. The angle of deviation from the orientation perpendicular to the direction of the tensile force was equal to 10°. In both cases shown in Fig. 14 the ratio ξ was equal to $\xi = 0.47$.

5. Conclusions

Basic continuum concepts concerning plastic deformation and the process of fracture have been in numerous works analysed in terms of microstructure of the material. Two-dimensional experimental models discussed in the present work allow us to demonstrate and study the possible contribution of the intercrystalline fracture and grain boundary sliding to the complex phenomena connected with the plastic deformation and fracture of polycrystalline metals. Since the mechanisms of grain boundary sliding and grain interior deformation are generally accepted to be mutually independent processes, it seems to be very convenient to analyse these mechanisms separately. In the models discussed in this work the grain interior deformation and transgranular fracture have been eliminated. The deformation of such artificial aggregates was connected with the sliding along boundaries between adjacent elements and the decohesion on these boundaries. The models demonstrate instability of the aggregate connected with the "intercrystalline" fracture and the influence of the grain size on the strength of the aggregate. The influence of the strength of the intercrystalline boundary on the mode of deformation of the aggregate has also been demonstrated.

References

1. F. GAROFALO, *Ductility in creep*, in: Ductility, papers presented at the seminar of the American Society for Metals 1967, ASM, Metals Park, Ohio 1968.
2. V. SKLENICKA, I. SAXL, J. POPULE, J. CADEK, *Strain components in high temperature creep of a* Cu-30% Zn *alloy*, Material Science and Engineering, **18**, 271–278, 1975.
3. B. DYSON, M. S. LOVEDAY, M. I. ROGERS, *Grain boundary cavitation under various states of stress*, Proc. Roy. Soc. London, A. 349, 245–259, 1976.
4. G. S. PISARENKO (editor), *Strength of materials and structural elements*, Naukova Dumka, vol. 1, p. 23, Kiev 1980 [in Russian].
5. D. A. KELLY, *A two-dimensional model of creep cavitation failure in copper subject to biaxial stress systems at* 250° C, Metal Science, 57–62, February 1976.
6. B. F. DYSON, *Constraints on diffusional cavity growth rates*, Metal Science, 349–353, October 1976.
7. D. C. DRUCKER, *Engineering and continuum aspects of high-strength materials*, Chapter 21 in: High Strength Materials, Edited by V. F. ZACKAY, Proc. 2nd Berkeley International Material Conference High-Strength Materials held in Berkley 1964 [J. Wiley].
8. C. S. BARRET, *Structure of metals*, Mc. Graw-Hill, New York 1952.

POLISH ACADEMY OF SCIENCES
INSTITUTE OF FUNDAMENTAL TECHNOLOGICAL RESEARCH.

Received February 12, 1982.